Microstructural investigation of the formation and development of topologically close-packed phases in a 3rd generation nickel-base single crystal superalloy

Kim, KeeHyun; Withey, Paul

DOI:
10.1002/adem.201700041

Microstructural investigation of the formation and development of topologically close packed phases in a 3rd generation nickel-base single crystal superalloy**

By *KeeHyun Kim*,* and *Paul Withey*

[*] *Dr.K. H. Kim, Prof. P.A. Withey*
School of Metallurgy and Materials, University of Birmingham
Birmingham, B15 2TT, UK
E-mail:k.kim.2@bham.ac.uk
Prof. P.A. Withey
Rolls-Royce plc, PO Box 31
Derby, DE24 8BJ, UK

[**] *The financial support and provision of evaluation test pieces by Rolls-Royce plc is acknowledged.*

Abstract: Topologically close-packed (TCP) phases, which degrade the creep and rupture properties of superalloys, generally form during long period aging or in-service. In this study, however, the early stage formation and development of TCP phases, which has received relatively less attention, was extensively investigated from as-cast samples through to fully heat-treated ones using high magnification and high resolution electron microscopy. TCP phases were surrounded with a γ′ phase, and their compositions were slightly different due to the structural and compositional complexity. In addition, even though TCP phases looked needle-shaped, the cross-section clearly showed that they were almost flat plates. Most of all, extremely fine particles of about 100 nm containing large amounts of rhenium formed in the early processing stages such as casting, solution heat treatment, or short aging. In addition, two different types of particles were detected at different formation stages: round-shaped particles at the starting point, and needle-like ones near the terminating point. Based on experimental observations, it was suggested that the needle-like particle probably showed the

growth of a TCP phase by the diffusion of rhenium after nucleation from a point containing high amounts of rhenium.

1. Introduction

Superalloys are one of the most advanced engineering high temperature materials showing excellent mechanical strength, creep, corrosion and oxidation resistance even close to their melting points, and they have found use in gas turbine engines, rocket components, nuclear reactors, industrial furnaces, and heat exchangers for jet propulsion and electricity generation.[1] As higher temperatures improve the efficiency of engines, more stable superalloys are continuously sought the application in the hottest parts of the engine in order to achieve the maximum turbine inlet temperature.[1a, 1d] For further improvement, a number of alloying elements are added to Ni-base superalloys and manufacturing processes such as the directional solidification of investment castings were developed to avoid the introduction of casting defects.[2]

As the strength and ductility of materials are basically governed by the way that atoms move past one another and dislocations move through grains, microstructural obstacles introduced by precipitation hardening and solid solution hardening can improve the mechanical behavior of metallic materials.[3] Therefore, the two different hardening methods are used to achieve the excellent high temperature properties of superalloys: precipitation hardening by a stable microstructure composed of a face-centered cubic structure matrix of γ phase and a fine dispersion of an ordered γ′ (Ni_3Al) phase, and solid solution hardening by the addition of a different soluble elements.[4] There are a number of investigations reporting the optimization of the size and morphology of the intermetallic γ′ phase,[5] and the effect of alloying elements in matrix strength.[1a, 1c, 1d, 6] It is well known that refractory alloying elements, such as niobium, molybdenum, tantalum, tungsten, and rhenium, enhance the high temperature creep

resistance and alloy stability.[1a] Among them, especially, the addition of rhenium increases the solidus and liquidus temperature of the nickel matrix, for example, the solvus temperature of Inconel 792 (0% Re) is 1100-1150 °C, but the temperature dramatically increases to 1305 °C in CMSX-4 (3% Re) and 1345 °C in CMSX-10 (6% Re).[1c] In addition, rhenium also increases the volume fraction of the γ′ phase. Most of all, the low solubility of rhenium in the γ′ phase makes it more effective than tantalum and tungsten in this role.[1c, 7] However, as the low diffusivity of rhenium in the nickel matrix can induce topological close packed (TCP) phases, the alloying content of Re in Ni-base superalloys is limited.

As most TCP phases degrade the creep and rupture properties of superalloys due to the depletion of the solid solution hardening elements in the matrix γ phase and enhance the accumulation of damage during deformation,[8] they have been continuously and widely investigated in order to minimize their formation since they were first discovered in the early 1960s.[9] Even though there are a number of publications describing the precipitation behavior of TCP phases,[9b, 10] there is little information on the original nucleation and development of TCP phases. Furthermore, it is known that TCP phases tend to occur near the surface of turbine blades where the surface has been aluminized and the local change in aluminum composition is sufficient to alter the local thermodynamics supporting the formation of TCP phases under the influence of high stress and thermal environment during in-service operations at high temperatures or long periods of aging [11]. In contrast, the early stage formation and development of TCP phases, such as during casting, solution heat treatment and short aging times, which is the other source of TCP formation related to the alloying elements in the base alloy, have not received the same level of investigation. Therefore, in this study, the early stage nucleation and development of TCP phases have been investigated from as-cast samples to fully heat-treated ones.

2. Experimental

A 3rd generation nickel-base single crystal superalloy (CMSX-10) was used to manufacture turbine blades at an aerospace production manufacturing facility. As shown in Table 1, the alloy has high amounts of alloying elements, especially rhenium. As-cast turbine blades were removed from the runner system and underwent solution heat treatment to generate the required microstructure of cuboids of γ′ phase in a matrix of γ phase. Due to the proximity of the γ′ solvus to the melting point, the solution heat treatment was slowly performed at 1316 °C for one hour; followed by two hour steps at 1329 °C, 1327 °C, 1340 °C, 1346 °C; then three hour steps at 1352 °C, 1357 °C, before slowing the heating rate to five hours at 1360 °C, ten hours at 1363 °C and finally fifteen hours at 1365 °C.[1c] After quenching from this heat treatment the blades were aged at 1100 °C for 4 hrs.

For microstructural investigation, the blades were cut out by wire-guided electro discharge machining (EDM), mounted and mirror-polished. Then, the polished samples were etched and ultrasonic-cleaned in ethanol for 5 min. A field emission scanning electron microscope (FE-SEM, FEI Quant 3D dual beam FIB-SEM) was used for general and ultra-high magnification observations, such as at ×100,000 and ×200,000, of TCP phases, as well as for chemical analysis using energy dispersive X-ray spectroscopy (EDX). After observation, cross-sectioning of regions of interest was performed by cutting and thinning using a focused ion beam (FIB) in the microscope. For high resolution and more precise chemical analysis, TEM samples were fabricated by an in-situ FIB lift-out technique [12], and observed using an FE transmission electron microscope (FE-TEM, FEI Tecnai F20) equipped with a scanning mode (STEM) and an EDX system. In this highly alloyed material it was difficult to distinguish clearly each element by SEM-EDX analysis [7a, 13] due to the close proximity of characteristic X-rays (M_α, keV) of alloying elements, such as Hf (1.644), Ta (1.709), W (1.774), and Re (1.842). In addition, the composition of phases in Ni-base superalloys showed local variations

due to precipitates.[7a] Therefore, the chemical analysis of samples was firstly checked by SEM, and then performed by TEM (precisely STEM-EDX with a nominal probe size of about 2 nm). The composition was acquired from more than 10 analysis areas to allow sufficient statistical confidence was provided by the Oxford AZtecTEM qualitative analysis software installed on the TEM. In order to avoid or minimize microstructural changes in the irradiated area,[12b] TEM samples were cooled with liquid nitrogen during TEM observation.

3. Results and Discussion

3.1 Typical morphology and composition of TCP phases

Figure 1 is a typical morphology of the TCP phases observed, which can be found in nickel-base single crystal superalloy turbine blades. In a plan view (Figs. 1a and 1d), the TCP phases look like needles on the surface of polished and etched samples, and show the brightest contrast even in a secondary electron (SE) image mode. A matrix γ phase and finely distributed precipitates of a γ′ phase show bright channels and dark background, respectively. These morphologies of TCP, γ, and γ′ phases have been well known. However, in order to observe the cross-section of TCP phases, a TCP phase was selected and cross-sectioned by FIB milling. As shown in Fig. 1c, it is clear that a tilting-view of the cross-section shows that the TCP phase is not a needle but an almost-flat plate. It is worth noting that in Figs. 1a-1c, as an etchant could attack preferentially γ′ phase, TCP phases as well as γ phase are visible clearly. On the contrary, in Figs. 1d and 1e, another etchant attacked TCP phases and γ phase, and consequently, a hollow needle-type morphology is visible. It is interesting to find that when the TCP phase was etched away a γ′ phase was seen surrounding the plate (see also Figs. 1b and 2). In order to confirm whether the etched-away part was a TCP phase, a protective platinum layer was deposited near the crossing point of two TCP plates (Fig. 1d) and cross-sectioned by FIB. A tilting view after the FIB cross-sectioning clearly shows that even though

the top parts were etched away, most of two TCP phases remain and as already shown in Fig. 1c, they are plates. Most of all, the tilting view (Fig. 1f) as well as the top views (Figs. 1a and 1d) of two crossing TCP plates indicate that even after two growing plates intersect, each TCP plate keeps its original growth direction without any bending or coalescence, which means the driving force for the growth of each TCP plate is extremely strong.

After the observation of two crossing TCP plates, a TEM sample was made exactly from the region. However, as both front and back sides of the region were milled away during TEM sampling by FIB, a STEM-HAADF image in Figure 2 shows two TCP plates close to their intersection, and this is a typical image of TCP plates which can be acquired by TEM. As already shown in previous SEM images (Figs. 1b and 1e), the TCP plates are definitely surrounded with γ′ phase. In addition, STEM-EDX element maps (Fig. 2b) show the distribution of each element near the TCP. Compared with γ′ and γ phases, high contrasts of Re, Cr, Co, W, Ta, and Mo display in the TCP plates. A spectrum (Fig. 2c) acquired by STEM-EDX point analysis on a TCP plate confirms that higher peaks of refractory elements, such as rhenium and tungsten. Based on the STEM-EDX point analysis, representative compositions of TCP plates as well as γ′ and γ phases are summarized in Table 1. The two TCP plates show slightly different compositions of Cr, Ta, and W. In order to confirm the difference, several other TCP plates were fabricated into TEM samples but all of them showed slightly different compositions (not reported here). After that, the compositions of the TCP plates were also compared with those of the most common TCP phases in Ni-base superalloys, such as σ, P, R, δ, μ, and M phases which were reported in literature [10a, 10d, 10e, 14]. However, it was confirmed that the compositions of TCP phases are different depending on the amounts of refractory metals in base materials as well as the manufacturing process, even in the same sample. In each TCP phase, numbers of atoms in the basis and coordination polyhedral, respectively, are σ(30, 10), P(56, 24), R(53, 27), δ(56, 24), μ(13, 7), and M(52,

38).[9b] In addition, the number of alloying elements in recently developed Ni-base superalloys can exceed ten. Therefore, considering the structural and compositional complexity of TCP phases, it is reasonable to suppose that each TCP has a slightly different composition.

3.2 Formation of TCP phases in early stage manufacturing processes

During manufacturing, as-cast Ni-based single crystal superalloy turbine blades undergo solution heat treatment and ageing to develop cuboids of γ′ phase in a matrix of γ phase. Therefore, to investigate the formation mechanism of TCP phases, it is necessary to know exactly when TCP phases begin to form.

Firstly, as-cast turbine blades were removed from the runner system and thoroughly scanned to find any TCP phases, but no TCP phases were observed. Secondly, as-cast turbine blades were just solution heat-treated and extensively investigated in order to find any TCP phases. Figure 3a is a representative SEM image of the solution heat-treated samples. It is clear that TCP phases can form only after exposure to high temperatures such as solution heat treatment. Thirdly, as-cast turbine blades were fully heat treated, receiving a solution heat treatment and subsequent short aging. Figure 3b is another representative SEM image of a fully heat-treated sample. When compared to the only solution heat-treated samples, it can be seen that more TCP phases form through the full heat treatment cycle the samples pass. These observations in solution heat-treated and fully heat-treated samples mean that TCP phases can exist even during the manufacturing of turbine blades (as well as after long period aging or in-service use) even though the amount of TCP phases present in the early stage is not great.

Considering the composition of TCP phases, it is known that TCP phases probably form in the matrix γ channels. In order to investigate their formation in these γ channels, a number of TEM samples were taken from candidate regions, such as dendritic cores and solidification grain boundaries. Figure 4 is a STEM-HAADF image and element maps showing the

formation of a TCP phase in a γ channel. A tiny TCP particle exists in the channel and connects two γ channels existing in the top and bottom regions in the image. In addition, when compared to the γ phase, the TCP shows brighter contrast due to larger amounts of refractory metals, such as Re and W. However, due to its morphology, it seems that the TCP phase in Fig. 4 had not just formed but had already grown after its initial formation in a γ channel.

3.3 Formation of Re-rich particles

As already described, TCP phases can form during turbine blade manufacture, which means that there is a possibility of TCP formation during casting although any fully formed TCP phases were not detected in the previous observation. Subsequently, as-cast turbine blades were re-scanned very slowly and thoroughly by SEM. Figure 5 shows an interesting finding in the dendritic regions of as-cast samples. At a relatively low magnification (×15,000), it appeared that there were some tiny particles in γ′ phase (Fig. 5a). At this magnification, however, it was difficult to observe the detailed microstructure of the particles. Much higher magnification images acquired at ×80, 000 (Fig. 5b) and at ×100,000 (Fig. 5c), respectively, clearly indicate that there are extremely fine particles inside the γ′ phase. In addition, a tilting view (Fig. 5d) of the particle observed at Fig. 5c indicates that the fine particle is not contamination adhered to the sample surface during sample preparation or observation.

At this stage, it was necessary to analyze the extremely fine particle, approximately 100 nm across, however, due to the inherit interaction volume of the X-ray beam with the sample, it was not precise enough to use the SEM-EDX system for the analysis. Therefore, an in-situ FIB lift-out technique was used to make a TEM sample containing the fine particle. Figure 6 shows the STEM images and STEM-EDX analysis (with a nominal probe size of 2 nm) of the fine particle. It should be noted that, due to the small size of the particle, it was difficult to fabricate a TEM sample, a thin lamellae containing the particle was left thicker than usual in

order to minimize the possibility of milling-away of the particle during TEM sampling by a strong gallium ion beam. In addition, as seen in Fig. 6a, the bottom part of the lamellae was also not thinned sufficiently. Nonetheless, STEM-HAADF images (Fig. 6a) clearly show that there is a fine and bright particle surrounded by a darker phase, which indicates that the particle is composed of heavier elements than nickel. A STEM-EDX element map of Re (Fig. 6b) strongly indicates a large amount of Re inside the fine particle. A spectrum (Fig. 6c) acquired by STEM-EDX point analysis indicates that the particle is mainly composed of Re and Ni. The composition of the particle acquired by a STEM-EDX point analysis was summarized in Table 1. The particle contains 50 at % Re, while the γ phase contains approximately 6 % Re (Table 1).

Our recent study also showed many fine rhenium-rich particles in solutioned and aged samples associated with solidification grain boundaries.[15] In addition, similar fine particles were also observed in just solution heat-treated samples (not included here). In order to compare the fine particles formed under different processing conditions, a sample showing a stray grain after solution heat-treatment and ageing, and then etched for visual inspection, was selected. Figure 7 is SEM and TEM images of a boundary region between the stray and matrix grains. After polishing and etching, the boundary was easily visible as shown in Fig. 7a. In addition, it is clear that there is an easily distinguishable layer about 4 μm across and composed of many elongated γ′ and γ phases (see also Ref. [15]). Most of all, the interface between this layer and the stray grain was coherent as seen by a good orientation match between them, while the interface between the layer and the matrix was sharp (not coherent), which is important in the understanding of the formation mechanism of the layer. For the layer formation, the activation energy should be reduced through the releasing of free energy which is related to a misfit strain energy per unit volume.[16] Consequently, it is necessary to achieve a good lattice match through a small disregistry along a specific plane, allowing the

nucleating and nucleated material having the same crystal structure and similar crystallography.[17] Therefore, the sharp interface was not the starting point of the formation of the layer, which means that the layer was formed from the coherent interface and terminated at the sharp interface.

It should be emphasized that many fine particles were detected only along the coherent interface as marked with arrows in Fig. 7a. After the SEM observation, a TEM sample was made exactly on the interface by an in-situ FIB lift-out technique in order to observe and analyze the particles. A higher magnification STEM-HAADF image (Fig. 7b) which was acquired after TEM sampling shows a fine particle which was detected in a layer between a stray and a matrix grains. The size and morphology of fine particles formed after solution heat-treatment and short aging is similar to the fine particles which were formed in the as-cast sample (Fig. 5). Most of all, the composition acquired from the particle by an STEM-EDX point analysis showed large amounts of Re (about 62 at%), which is similar to that of the particle in Fig. 6 and Table 2 (see also Ref. [15]). This observation suggests that the fine particles containing large amounts of Re can form at any processing stage, i.e. during casting, solution heat treatment, or short aging.

A supersaturated solid solution in Ni-base superalloys generates finely distributed precipitates of a γ′ phase during heat treatment, and TCP phases form during in-service or prolonged heat treatments. In addition, it is known that, when a TCP phase formed, TCP-forming elements were probably depleted from the general microstructure near the TCP phase. However, as shown in Table 1, the composition of γ′ phase surrounding TCP plates was almost the same as the γ′ phase in the general matrix. In other words, the depletion of TCP-forming elements was not observed. In addition, each TCP plate was always surrounded by the γ′ phase of approximately 500 nm thickness, which was almost the same as only one or two layers of γ phase. Therefore, it is difficult to explain the formation of a TCP plate

surrounded with one layer of γ phase with the depletion mechanism of TCP-forming elements. Instead, considering similar compositions of γ′ phases near TCP phases or inside matrix, it can be suggested that from a supersaturated matrix, excessive rhenium atoms over a solubility limit can be diffused out and form Re-rich particles during casting or heat treatment, and then may develop into TCP phases.

3.4 Development of TCP phases

As shown in Fig. 7a, there are many fine particles at the coherent interface between two grains. After detection of the particles a cross-section was serial-milled along the interface in order to investigate further the distribution and morphology of the fine particles. Figure 8a is a top-view after initial cross-sectioning of the intermediate layer formed between a stray and a matrix grains. It should be noted that the direction of the cross-section is along the interface. A protective platinum layer was deposited on the selected region to protect it during FIB serial milling as marked with an arrow in the figure. A tilting view of the cross-section (Fig. 8b) shows that there are also many needle-like particles in γ′ and γ phases. Most of all, it should be emphasized that the needle-like morphology of the particles are completely different from the round-shaped particles which were shown in Fig. 7, which means that two different types of particles were detected in the same sample and within the same intermediate layer. In the two figures (Figs. 7a and 8b), the only difference was the direction of SEM observation: top-view near the layer (Fig. 7a), and tilting-view after cross-sectioning along the layer (Fig. 8b). Then, the cross-section was further milled and observed as shown in Fig. 8c. It is interesting to find from the cross-section that the two different types of particles co-exist at the same area as marked with arrows. Figure 8d is another tilting view of the cross-section after the final serial-milling. Only several round-shaped particles are visible near the top surface because most of the intermediate layer below the top surface was milled away and

consequently, the matrix grain was revealed and observed as shown in Fig. 8d. It means that the particles exist only in the boundary layer between stray and matrix grains.

In the previous section, it was shown that the round-shaped particles contain large amounts of Re, more than 60 at %. Most of all, regardless of the analysis point by STEM-EDX, the composition of the particle is uniform as summarized in Table 2. Then, it was necessary to investigate the needle-like particles, however, as their size was too small to analyze using SEM, TEM samples were fabricated exactly from the area shown by FIB milling. Figure 9 is a representative TEM image showing a needle-like particle. When compared to the TEM image of a round-shaped particle (Fig. 7b), the different morphology of the needle-like TCP particle is obvious. In addition, the needle-like particle is surrounded by γ′ phase. A STEM-EDX line profile was carried out on the particle, Fig. 9b, and it clearly shows that the composition of the needle-like particle continuously changed along the particle length. Three representative compositions acquired on the particle were summarized in Table 2. In the three analyses the amounts of Re in the needle-like particle were approximately 45, 54, and 63 %, depending on the analysis point, whereas the amounts of Re in the round-shaped particle was almost uniform at 60 % regardless of analysis points. In addition, as previously discussed, the intermediate layer containing the particles started to grow from the coherent interface and terminated at the sharp interface (Fig. 8), which means that the round-shaped particles exist at the starting point for the formation the layer and on the contrary, the needle-like particles only exist at the middle of the layer or near the terminating point. This observation suggests that the needle-like particle probably shows a growth stage, i.e. the growth of a TCP phase by the diffusion of Re after nucleation from a region containing high amounts of Re or the rejection of Re from the γ' phase as there is no solubility of Re in γ'.

In order to investigate the possibility of the growth of TCP phases through the diffusion of Re, a number of Ni-base single crystal turbine blades were observed. Figure 10 shows the

evidence for the diffusion of Re. At the dendrite core, large amounts of Re was clearly detected, whereas the amounts of Re were dramatically decreased at the dendrite arms. Considering the interaction volume of the incident X-ray beam in SEM-EDX analysis with the sample surface, the accuracy of the composition at each point by SEM-EDX might not be reliable. However, if the composition on each point were an artifact, the dendrite core with the smallest size (see Figs. 10b and 10c) should have shown the smallest amount of Re, whereas the dendrite arms with bigger size should have shown the highest amounts. Therefore, even though considering the interaction volume of the inherent SEM-EDX analysis, the composition on each point indicates a reliable trend and shows the diffusion of Re from the dendrite core into the dendrite arms.

However, although the diffusion of Re was confirmed, there was not any direct evidence of the growth of TCP phases. Therefore, a number of TCP plates were carefully observed again to find any evidence. At this stage, it is necessary to remember that the morphology of TCP phases observed was almost a flat plate as shown in Figs. 1-3. However, an SEM image (Fig. 11a) acquired from a TCP plate shows something different. A higher magnification image (Fig. 11b) clearly shows that the TCP phase is not completely flat; it can be noted that the centre region is thicker than the edges. Therefore, this observation suggests that after a TCP phase was formed from the central region in Fig. 11.b, and subsequently it was grown by the diffusion of Re and finally formed the observed morphology. Finally, it is also suggested that excessive alloying elements over solubility limits exist in a supersaturated matrix, and after the formation of TCP or Re-rich particles, they diffuse into the TCP or Re-rich particles.

Based on these observations, a schematic diagram is proposed (Fig. 12). In a supersaturated matrix, excessive rhenium, over a solubility limit, diffuses and forms Re-rich particles. At the same time, in a γ channel, a fine particle is also precipitated (Fig. 12a). After that, TCP phases are continuously grown by the diffusion of rhenium (Figs. 12b and 12c). Even though the

growing TCP plates meet at one point, they keep their original growing directions due to the strong driving force (12d).

4. Summary

TCP phases which were found in nickel-base single crystal superalloy turbine blades were observed using high resolution electron microscopy. Even though TCP phases looked needle-shaped, the cross-section clearly showed that they were in fact flat plates. Two crossing TCP plates kept their original growth directions without any bending or coalescence due to the extremely strong driving force for their growth along certain crystallographic planes. These TCP phases were surrounded by a γ′ phase, and their compositions were slightly different to each other due to their structural and compositional complexity. Interestingly, the composition of the γ′ phase surrounding a TCP phase was almost uniform without showing the depletion of TCP-forming elements.

Extremely fine particles (about 100 nm across) containing large amounts of rhenium formed in manufacturing stages for turbine components, i.e. during casting, solution heat treatment, or short aging. A TEM element map of rhenium indicated a large amount of rhenium inside the fine particles. In addition, two different types of particles were detected in an intermediate layer which grew from a coherent interface and terminated at a sharp interface: round-shaped particles at the starting point for the formation the layer, and needle-like particles at the middle of the layer or near the terminating point. This observation suggested that the needle-like particle probably showed similar growth characteristics to a TCP phase through the diffusion of Re after nucleation from a point containing high amounts of Re. From a supersaturated matrix, excessive rhenium atoms, over a solubility limit, were probably diffused out and formed Re-rich particles during casting or heat treatment, and then may be sites which later developed into TCP phases. In order words, TCP phases with the size of

approximately 100 nm formed in γ channels or from Re-rich particles inside γ′ phases during heat treatment, would develop into typical TCP plates with the size of about 30 μm. Finally, even though TCP phases usually formed during long period aging or in-service, this study clearly showed that they could form even in the early stages of manufacturing of turbine blades with low amounts of TCP phases in the early stages. Therefore, it would be required to investigate the formation and development of TCP phases from the early stages of manufacturing processes for better understanding of these advanced engineering materials and better control of TCP phases.

References

[1] a) M. Durand-Charre, *The microstructure of Superalloys*, OPA, Amsterdam **1997**; b) Y. Bar-Cohen, *High Temperature Materials and Mechanisms*, CRC Press, New York **2014**; c) B. Geddes, H. Leon, X. Huang, *Superalloys : alloying and performance*, ASM International, Materials Park, Ohio **2010**; d) R. C. Reed, *The superalloys : fundamentals and applications*, Cambridge University Press, Cambridge **2006**.

[2] T. M. Pollock, S. Tin, *J. Propul. Power* **2006**, 22, 361.

[3] T. J. Rupert, D. S. Gianola, Y. Gan, K. J. Hemker, *Science* **2009**, 326, 1686.

[4] W. J. Molloy, *Advanced materials and Processes* **1990**, 138, 23.

[5] G. Brewster, H. B. Dong, N. R. Green, N. D'Souza, *Metallurgical and Materials Transactions B* **2008**, 39, 87.

[6] W. F. Smith, *Structure and Properties of Engineering Alloys*, McGraw-Hill Book Co., **1994**.

[7] a) P. J. Warren, A. Cerezo, G. D. W. Smith, *Materials Science and Engineering: A* **1998**, 250, 88; b) A. F. Giamei, D. L. Anton, *MTA* **1985**, 16, 1997; c) A. C. Yeh, S. Tin, *Scripta Materialia* **2005**, 52, 519.

[8] a) M. V. Acharya, G. E. Fuchs, *Materials Science and Engineering: A* **2004**, 381, 143; b) A. Volek, F. Pyczak, R. F. Singer, H. Mughrabi, *Scripta Materialia* **2005**, 52, 141; c) M. Simonetti, P. Caron, *Materials Science and Engineering: A* **1998**, 254, 1.

[9] a) S. T. Wlodek, *Trans. ASM* **1964**, 57, 110; b) B. Seiser, R. Drautz, D. G. Pettifor, *Acta Materialia* **2011**, 59, 749.

[10] a) K. Matuszewski, R. Rettig, H. Matysiak, Z. Peng, I. Povstugar, P. Choi, J. Müller, D. Raabe, E. Spiecker, K. J. Kurzydłowski, R. F. Singer, *Acta Materialia* **2015**, 95, 274; b) X. P. Tan, H. U. Hong, B. G. Choi, I. S. Kim, C. Y. Jo, T. Jin, Z. Q. Hu, *Journal of Materials Science* **2013**, 48, 1085; c) S. Tin, T. M. Pollock, *Materials Science and Engineering: A* **2003**, 348, 111; d) A. Volek, R. F. Singer, R. Buergel, J. Grossmann, Y. Wang, *Metallurgical and Materials Transactions A* 37, 405; e) C. M. F. Rae, M. S. Hook, R. C. Reed, *Mater. Sci. Eng. A-Struct. Mater. Prop. Microstruct. Process.* **2005**, 396, 231; f) S. Gao, Y. Z. Zhou, C. F. Li, J. P. Cui, Z. Q. Liu, T. Jin, *Journal of Alloys and Compounds* **2014**, 610, 589; g) E. N. Kablov, N. V. Petrushin, M. B. Bronfin, A. A. Alekseev, *Russian Metallurgy (Metally)* **2006**, 2006, 406.

[11] M. Clancy, M. J. Pomeroy, *Metall. Mater. Trans. A-Phys. Metall. Mater. Sci.* **2013**, 44A, 3028.

[12] a) K. Kim, M. Watanabe, J. Kawakita, S. Kuroda, *Scripta Materialia* **2008**, 59, 768; b) K. Kim, *Metallurgical and Materials Transactions A* **2014**, 45, 3650.

[13] JEOL, Energy table for EDS analysis, http://www.jeol.com, accessed: September 28, 2013.

[14] a) R. W. Broomfield, Ford, D. A., Bhangu, J. K.,Thomas, M. C.,Frasier, D. J.,Burkholder, P. S.,Harris, K.,Erickson, G. L.,Wahl, J. B., *Journal of Engineering for Gas Turbines and Power* **1998**, 120, 595; b) C. M. F. Rae, R. C. Reed, *Acta Materialia* **2001**, 49, 4113; c) F. Ritzert, D. Arenas, D. Keller, V. Vasudevan, *The effect of alloying on topologically close packed phase instability in advanced nickel-base superalloy Rene N6*, Minerals, Metals & Materials Soc, Warrendale **1998**; d) W. S. Walston, J. C. Schaeffer, W. H. Murphy, *A new type of microstructural instability in superalloys - SRZ*, Minerals, Metals & Materials Soc, Warrendale **1996**; e) Q. Feng, T. K. Nandy, T. M. Pollock, *Materials Science and Engineering: A* **2004**, 373, 239; f) Q. Feng, T. K. Nandy, S. Tin, T. M. Pollock, *Acta Materialia* **2003**, 51, 269.

[15] K. Kim, P. Withey, W. D. Griffiths, *Metallurgical and Materials Transactions A* **2015**, 46, 1024.

[16] D. A. Porter, K. E. Eastering, M. Y. Sherif, *Phase transformations in metals and alloys*, CRC Press, Boca Raton **2009**.
[17] a) K. Nogita, S. D. McDonald, K. Tsujimoto, K. Yasuda, A. K. Dahle, *J. Electron Microsc.* **2004**, 53, 361; b) H. S. Dai, X. F. Liu, *Materials Science and Technology* **2009**, 25, 1183; c) B. Bramfitt, *Metallurgical Transactions* **1970**, 1, 1987.
[18] G. L. Erickson, *The development and application of CMSX (R)-10*, **1996**.

Figures and Figures captions

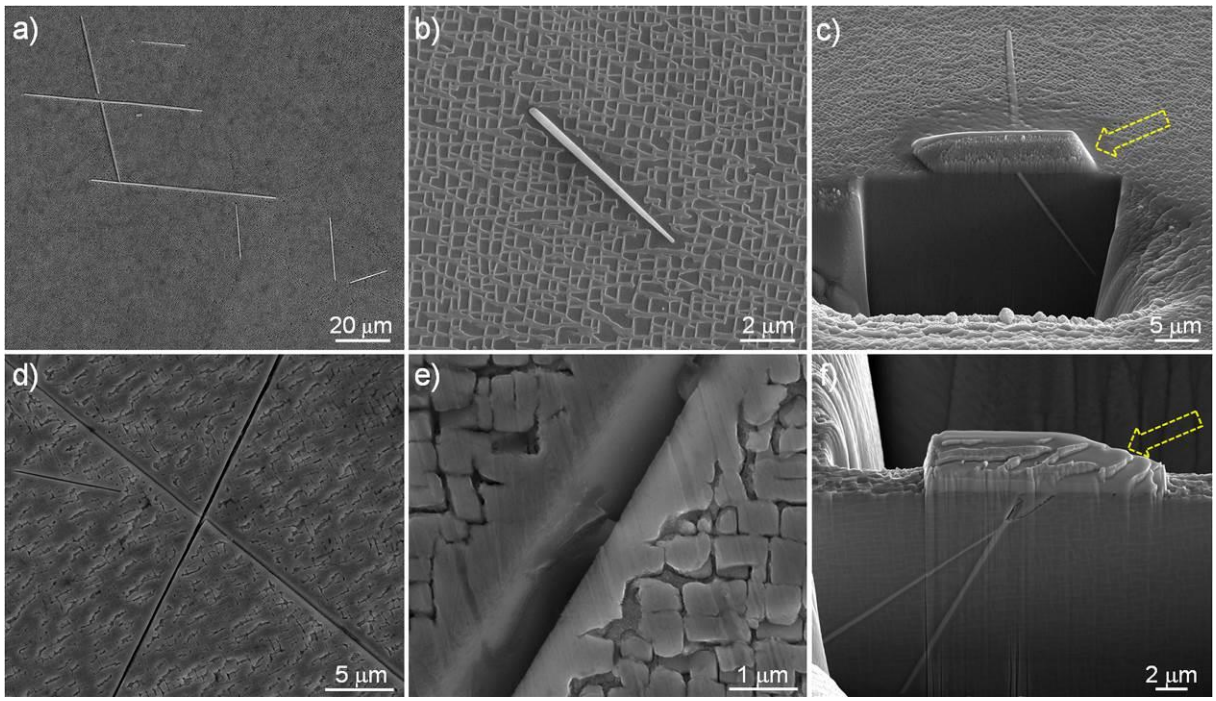

Fig. 1. Typical morphology of TCP phases observed by SEM: a) low magnification image showing several TCP phases, b) higher magnification image of a TCP phase, c) tilting-view showing the cross-section of a TCP phase, d) two-crossing TCP, e) close observation near a TCP phase, and f) tilting view of two-crossing TCP after FIB milling. The arrows in panel (c) and (f), respectively, indicate a protective platinum layer deposited on a TCP phase before cross-sectioning. Note that two different etchants could attack different phases, such as γ′ phase in a-c), and TCP phases in d-f), respectively.

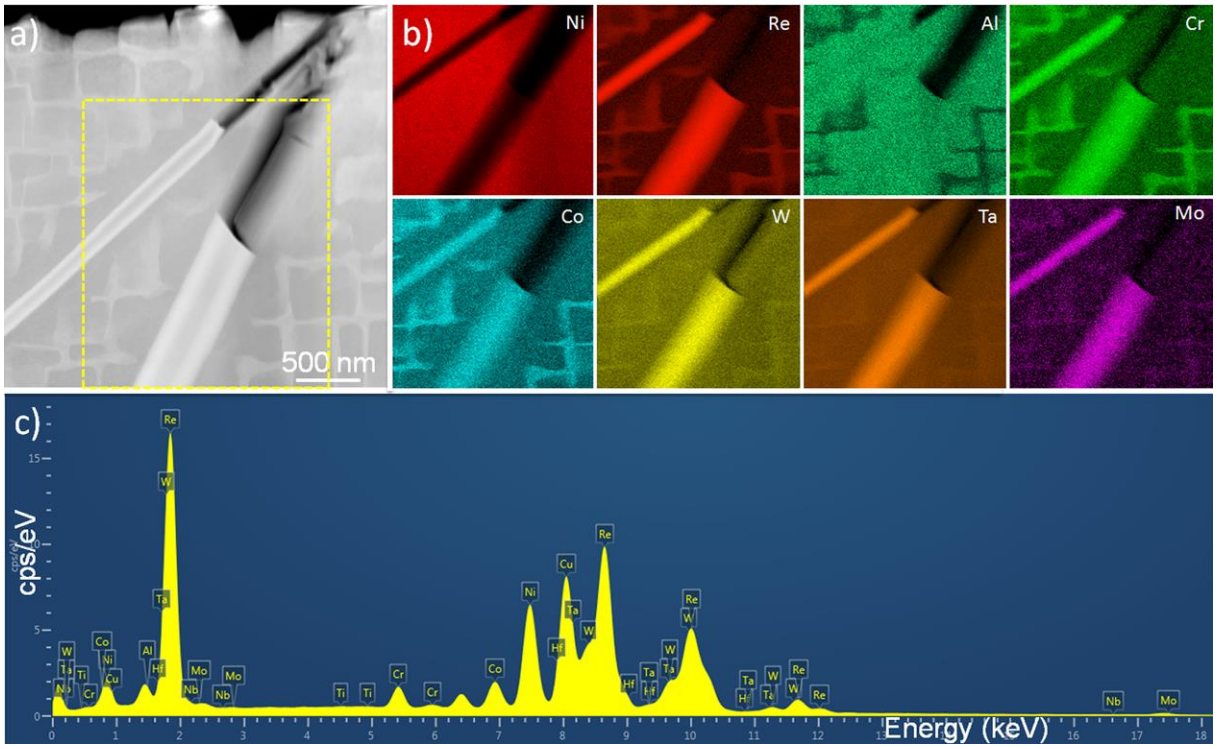

Fig. 2. Typical morphology of TCP phases observed by TEM: a) STEM-HAADF image showing two TCP phases, b) STEM-EDX element maps corresponding to the marked area in panel (a), and c) STEM-EDX point analysis on a TCP phase.

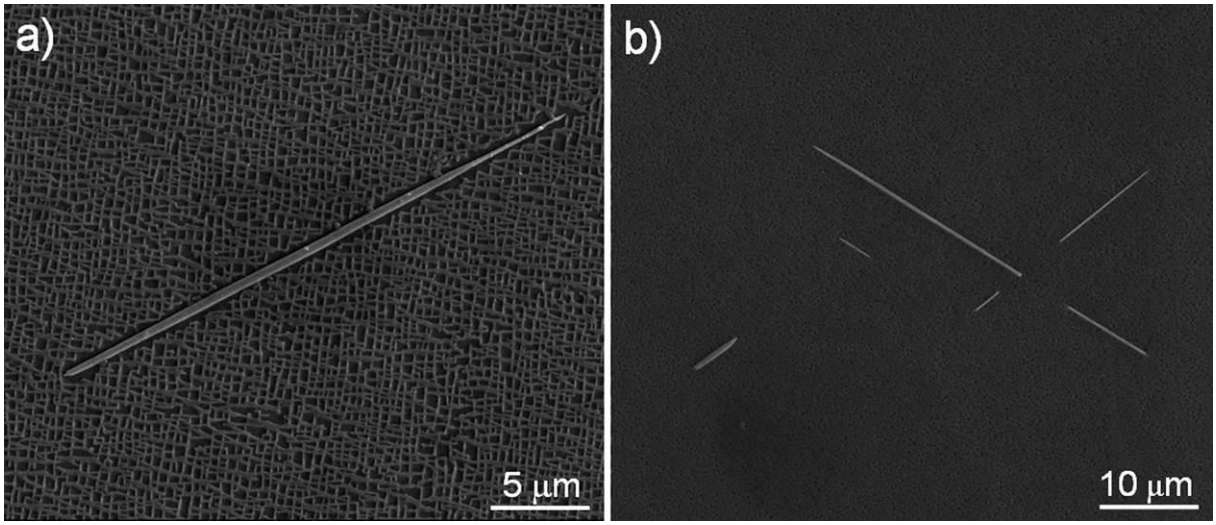

Fig. 3. Representative SEM images of an only solution heat-treated sample (a), and a fully heat-treated (solution heat-treatment and short aging) sample (b).

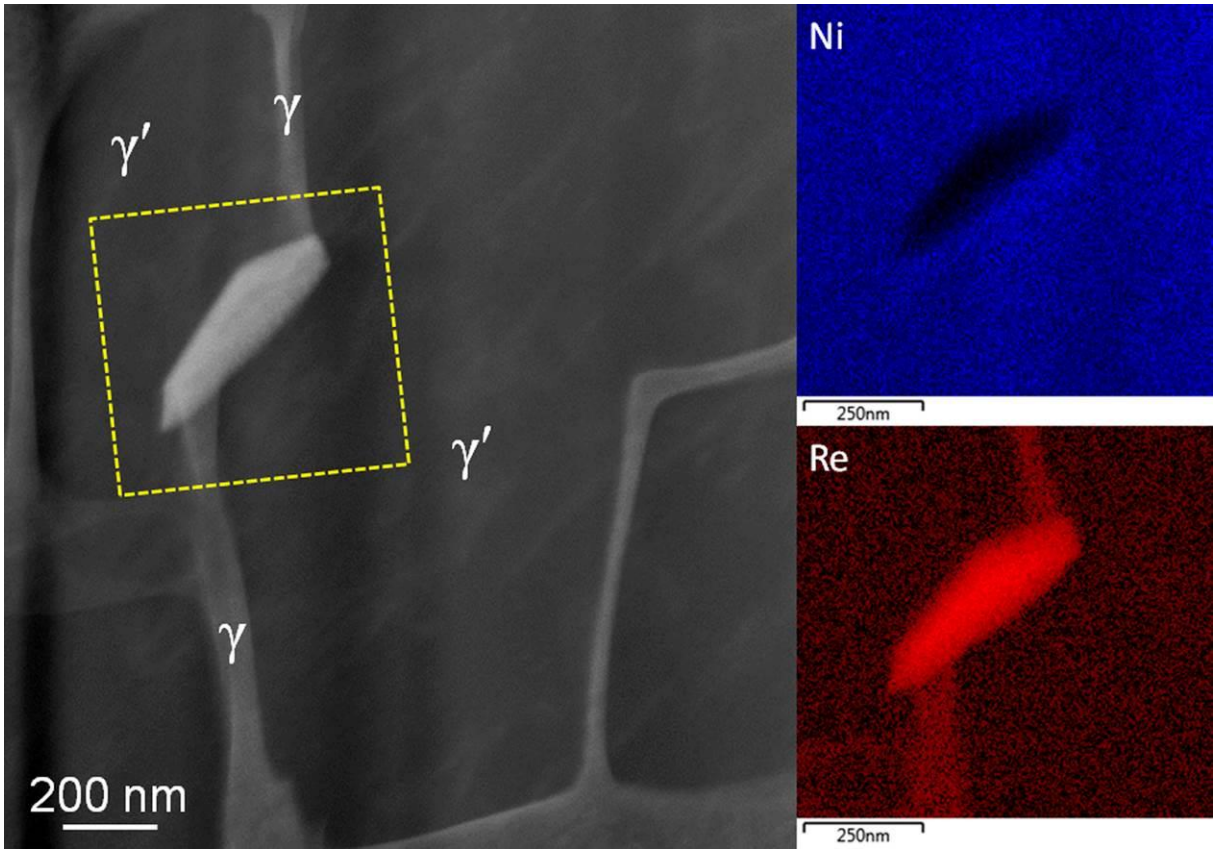

Fig. 4. A STEM-HAADF image and STEM-EDX element maps of nickel and rhenium at the marked region showing the formation of a TCP phase in a γ channel.

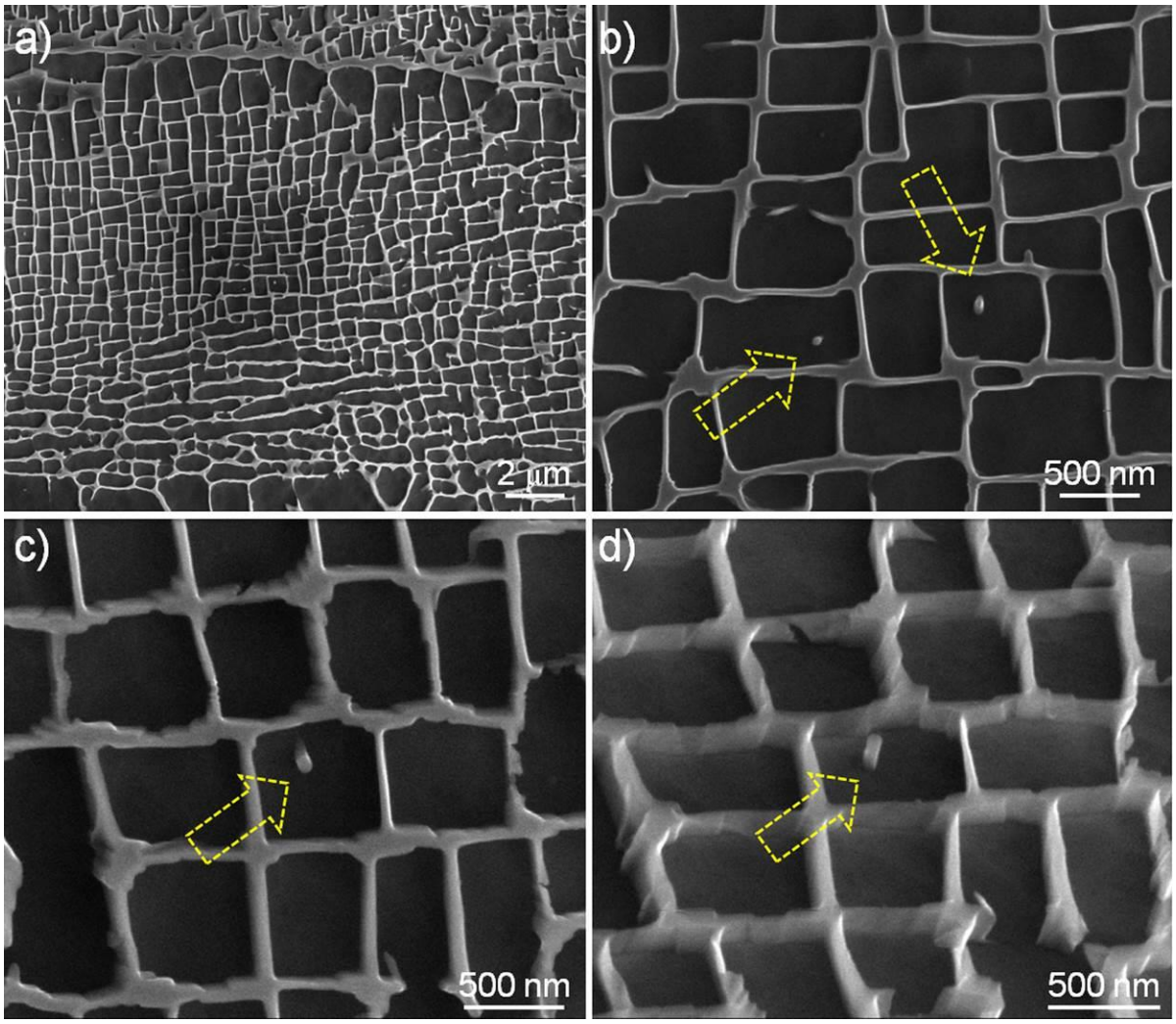

Fig. 5. SEM images showing several fine particles in an as-cast sample: a) low magnification image at an interdendritic region, b) higher magnification image of panel a), and c-d) one set images showing a particle of top view (c) and tilting view (d).

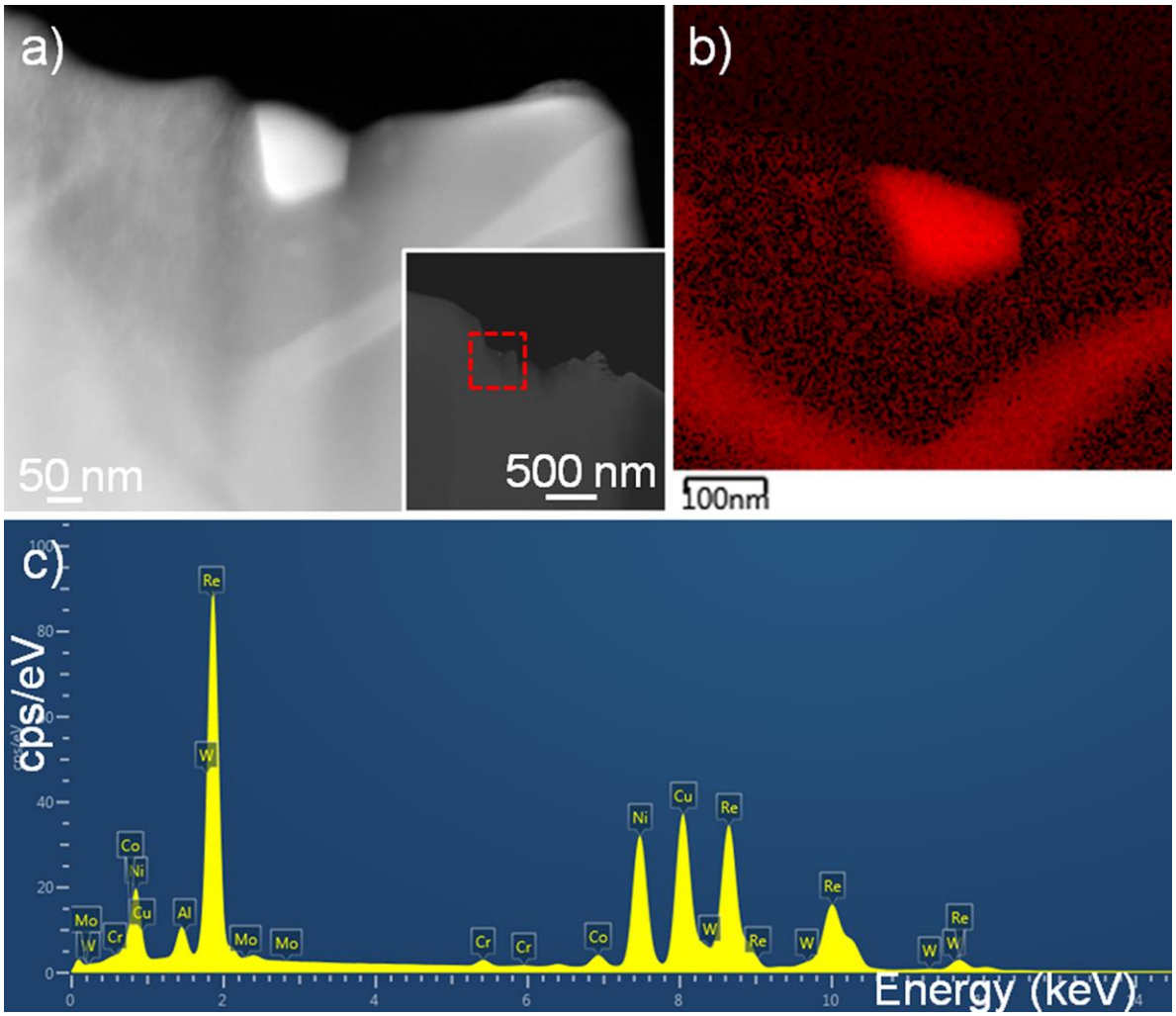

Fig. 6. STEM images and STEM-EDX analysis of the fine particle detected in Fig. 5: a) STEM-HAADF image with an inset of a general image, b) STEM-EDX element map of Re, and c) STEM-EDX spectrum.

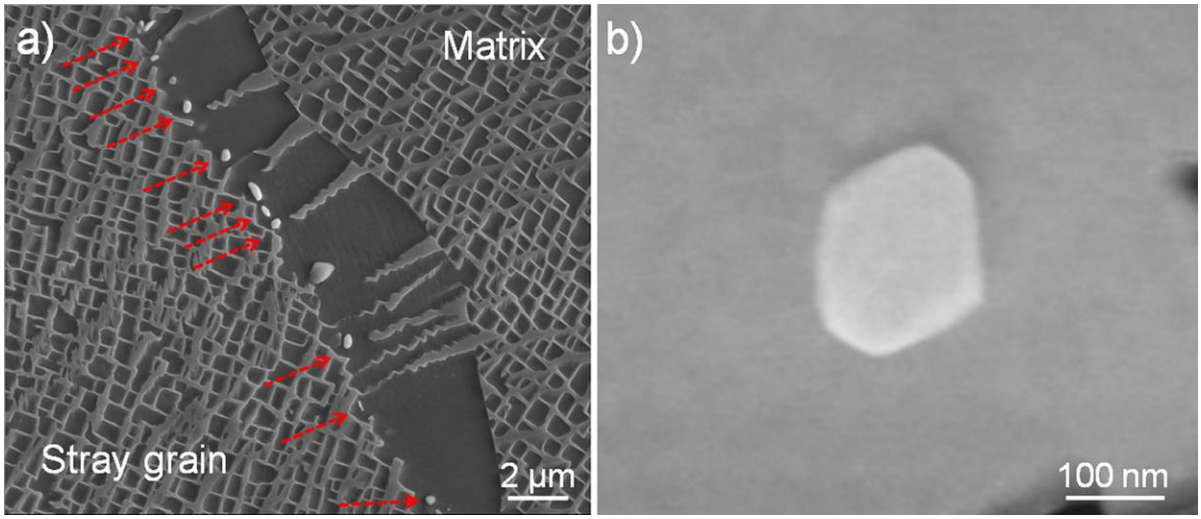

Fig. 7. SEM and TEM images of a boundary region between the stray and matrix grains: a) SEM top-view image near the interface between matrix and a stray grain (a), and b) STEM-HAADF image of a fine particle in (a) observed by TEM after TEM sampling exactly on the interface by an in-situ FIB lift-out technique. The arrows in (a) indicate fine particles along the coherent interface.

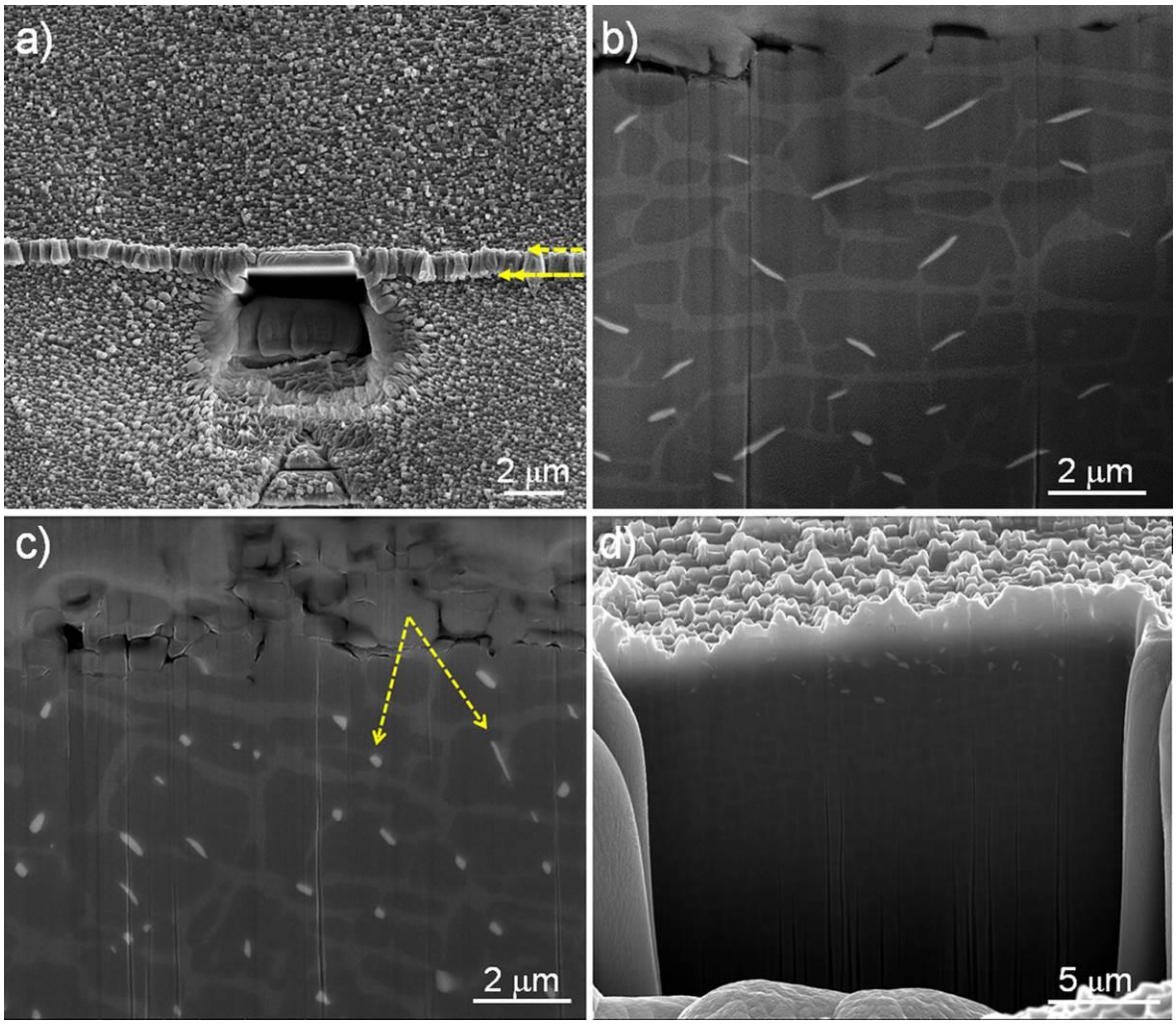

Fig. 8. SEM images of an intermediate layer formed between a stray and a matrix grains and its cross-sections: a) top-view of a selected region after deposing a protective platinum layer and initial cross-sectioning, b) tilting-view of (a), c) another tilting-view after further milling, and d) final tilting-view after final milling showing round-shaped particles only near the top surface. Note that the intermediate layer in panel (a) containing the particles started to grow from the coherent interface (top side) marked with a single arrow and terminated at the sharp interface (bottom side) marked with a double arrow. In panel (d), most of the intermediate layer below the top surface was milled away and consequently, the matrix grain was revealed.

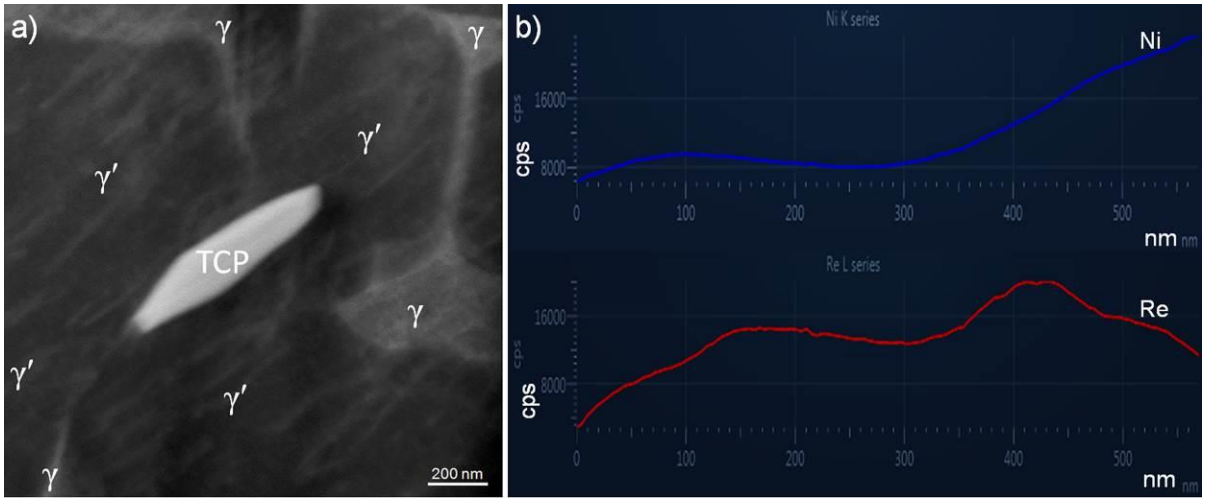

Fig. 9. TEM observation and analysis of a needle-like particle: a) STEM-HAADF image, and b) STEM-EDX element line profile along the TCP particle in (a).

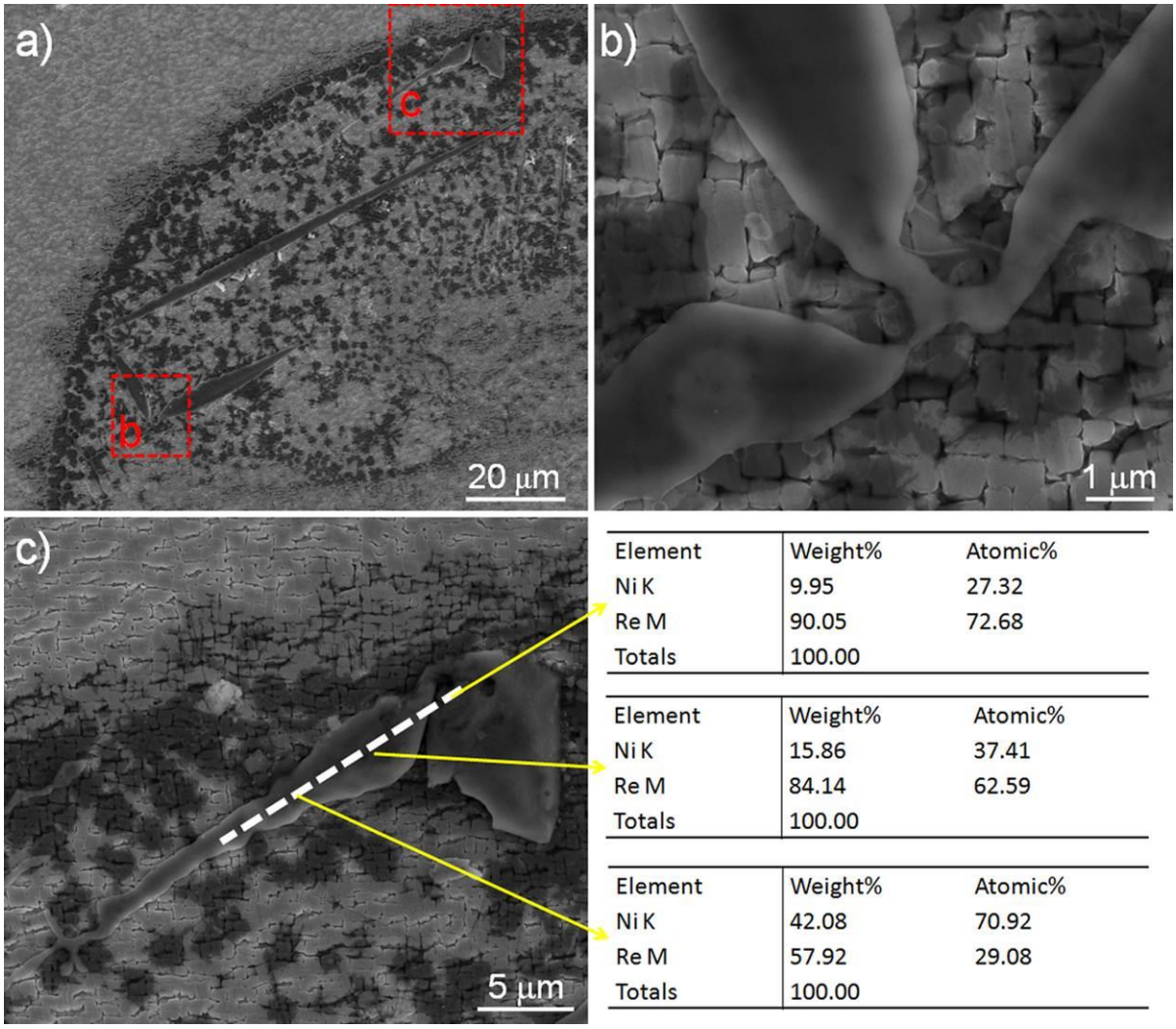

Fig. 10. SEM images and SEM-EDX analysis showing the diffusion of rhenium element: a) low magnification image, and b-c) close images at the marked regions in panel a), respectively. Note that, for simplicity, only the compositions of main elements such as Ni and Re were displayed along the line in (c)

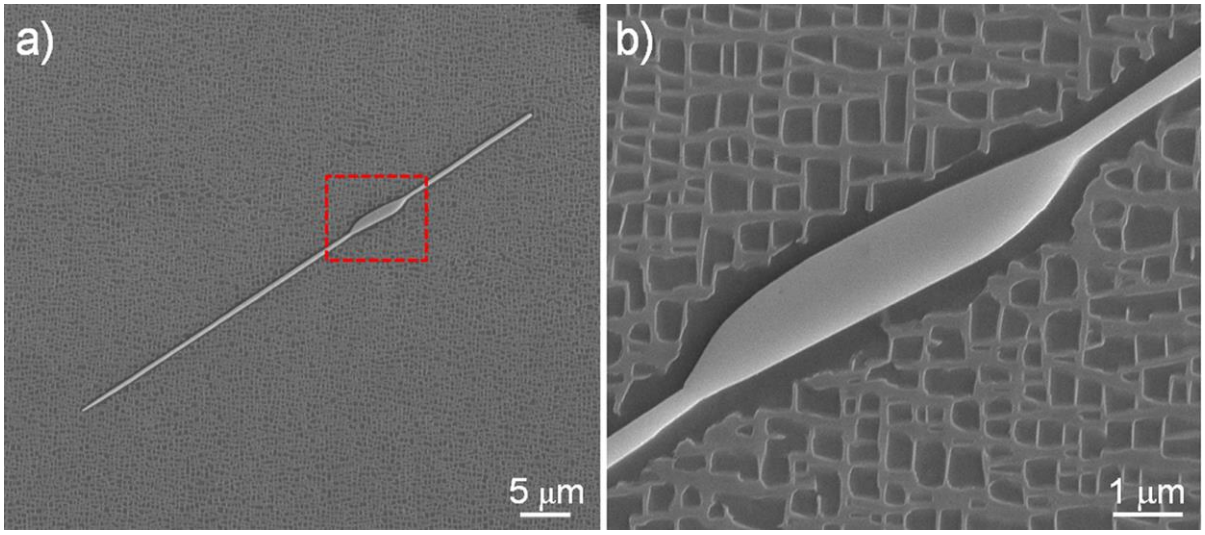

Fig. 11. SEM images showing the transition of a TCP phase: a) whole image of a TCP phase, and b) close observation at the marked region in (a).

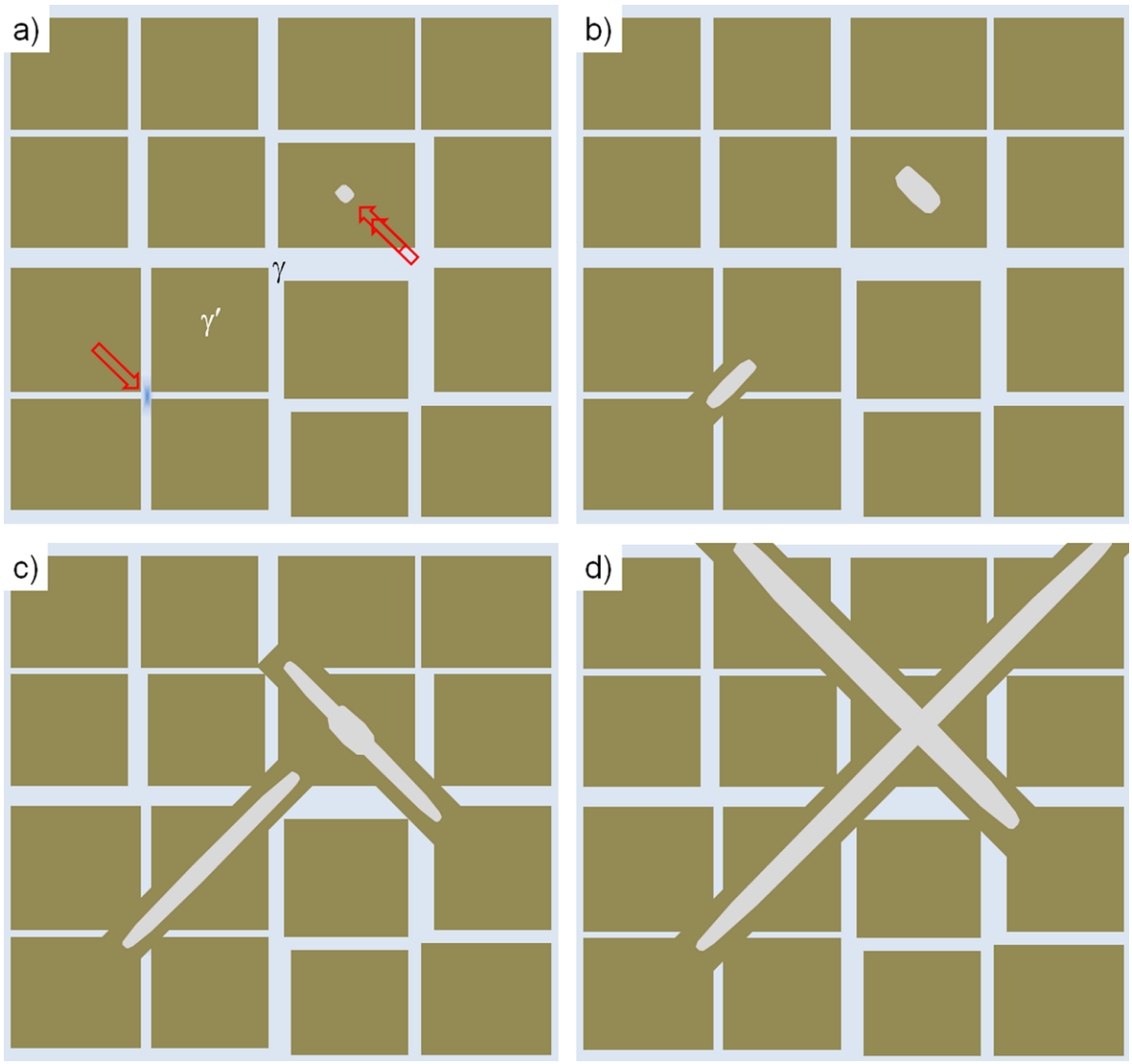

Fig. 12. A schematic diagram showing the nucleation and growth of TCP phases at four different stages: a) nucleation of fine particles in γ′ phase and γ channel, b-c) continuous growth of fine particles, and d) intersection of two growing TCP plates.

Table 1. Compositions of base materials [15, 18] and several phases including TCP measured by STEM-EDX

Element	Base	Re-rich after HT	Re-rich in as-casted	TCP	γ′ near TCP	γ′ in matrix	γ in matrix
Al	13.6	2.5	2.4	2.42	16.07	15.64	6.34
Ti	0.1	0.1	0.0(0.04)	0.11	0.13	0.13	0.00
Cr	1.8	1.7	1.9	3.95	0.86	0.97	4.07
Co	3.2	3.8	4.1	6.34	2.63	2.73	5.88
Ni	73.6	22.8	35.8	24.10	73.17	73.49	70.52
Nb	0	0	0.0	0.00	0.00	0.00	0.00
Mo	0.3	3.0	2.6	0.56	0.00	0.00	0.31
Ta	3.0	0.7	0.6	5.19	4.69	4.62	3.55
W	1.9	3.8	3.5	16.19	2.43	2.42	3.41
Re	2.4	61.6	49.1	40.99	0.02	0.00	5.91
Total	100	100	100	100	100	100	100

Table 2. Compositions of two different types of TCP particles measured by STEM-EDX

	Round-shaped particle			Needle-like particle		
Element	Point A	Point B	Point C	Point D	Point E	Point F
Al	2.22	2.30	2.19	4.52	2.67	2.16
Ti	0.00	0.00	0.23	0.04	0.06	0.00
Cr	1.85	1.80	1.77	1.81	1.99	1.83
Co	4.01	3.93	4.03	4.19	4.92	4.15
Ni	27.18	27.06	26.87	41.05	31.53	23.30
Nb	0.32	0.50	0.41	0.00	0.50	0.65
Mo	0.44	0.70	0.37	0.34	0.82	0.83
Ta	0.50	0.52	0.61	0.57	0.50	0.42
W	3.19	2.84	3.13	2.36	3.38	3.66
Re	60.29	60.36	60.39	45.11	53.64	63.01
Total	100	100	100	100	100	100